Talanta 119 (2014) 144–150

Contents lists available at ScienceDirect

Talanta

journal homepage: www.elsevier.com/locate/talanta

Optically encoded nanoprobes using single walled carbon nanotube as the building scaffold for magnetic field guided cell imaging

Hong Wang [a], Zhuyuan Wang [b,*], Minglang Ye [b], Shenfei Zong [b], Mingyue Li [b], Peng Chen [b], Xueqin Ma [b], Yiping Cui [b,*]

[a] Department of Laboratory Medicine, the First Affiliated Hospital of Nanjing Medical University, Nanjing 210029, China
[b] Advanced Photonics Center, Southeast University, Nanjing 210096, China

ARTICLE INFO

Article history:
Received 9 August 2013
Received in revised form
18 October 2013
Accepted 20 October 2013
Available online 30 October 2013

Keywords:
Surface enhanced Raman scattering
Fluorescence
Optical encoding
Carbon nanotubes
Magnetic field
Cell imaging

ABSTRACT

We construct a novel fluorescent, surface enhanced Raman scattering (SERS) encoded and magnetic nanoprobe for live cell imaging. To fabricate this nanoprobe, single walled carbon nanotube (SWNT) is used as the building scaffold while gold nanoparticles (Au NPs), superparamagnetic iron oxide nanoparticles (SPIONs) and quantum dots (QDs) are employed as the building blocks. Here, Au NPs serve as the SERS substrate and QDs act as the fluorescent agent. Au NPs and SPIONs are first adsorbed on the SWNT via electrostatic interactions. Then a silica layer is coated on the SWNT. Finally, QDs are attached on the silica shell. With such a structure, various optical signals can be readily encoded to the nanoprobe simply by using different Raman molecules and QDs with different emission wavelengths. Experimental results show that the as-prepared nanoprobe exhibits well fluorescence and SERS performance. Furthermore, *in vitro* experiments demonstrate that the nanoprobe can fulfill magnetic field guided fluorescence and SERS dual mode imaging of live cells. As a fascinating optical encoding material and a multifunctional nanoplatform, the presented nanoprobe holds genuine potential in future biosensing applications.

1. Introduction

The integration of various functions into a single platform is a thriving research area as it allows simultaneous accomplishment of different tasks [1,2]. As one of the particular nanosized platforms, composite nanoprobes have received massive attention concerned with their fabrication and utilization [3]. Such nanoprobes can be validly applied *in vitro* or *in vivo* due to their small size. Popular materials involved in the construction of nanoprobes include metal nanoparticles (NPs) [4], silica NPs [5], polymers [6], magnetic NPs (MNPs) [7], carbon nanotubes (CNTs) [8], liposomes [9], oligonucleotides [10] and so on. Among these, CNTs are attractive candidates due to their special chemical and physical characteristics, such as large surface area, high mechanical strength, excellent chemical and thermal stability and rich electrical and optical properties [11]. To date, CNTs have been implicated in biomedical studies, including drug delivery [12], cell endoscope [13], immunoassay [14], and photothermal therapy [15,16]. Aside from CNTs, another interesting and promising material is MNPs. Owing to their intrinsic magnetic property, MNPs can be facilely manipulated by an external magnetic field and realize magnetic field guided tumor specific drug delivery or cancer cell imaging [17–19]. Superparamagnetic iron oxide nanoparticle (SPION) with diameter of around 12 nm is one of the commonly used MNPs. With such a tiny size, they can be incorporated into other nanomaterials to form multifunctional nanocomposites [20,21].

A newly emergent kind of multifunctional nanoplatform is the optically encoded nanoprobe, which has been proven to have great applicability in bioimaging and biosensing [22,23]. Fluorescence is well employed in designing optical nanoprobes due to its fast readout and easy operation. Another involved technique is surface enhanced Raman scattering (SERS) as it has good multiplexing ability and can provide rich spectroscopic information of the analyte [24,25]. Despite their impressive progress, nanoprobes encoded with solely fluorescence or SERS signal still suffer from some annoying shortcomings. For example, the wide bandwidth of fluorescence often causes severe spectral overlap, which limits the multiplexing ability of fluorescence technology. While SERS usually requires a relatively long acquisition time due to its weak signal intensity, which hinders its application in high-speed dynamic analysis. As a result, combining both SERS and fluorescence into a single nanoprobe can be an effective solution. Several such SERS and fluorescence dual encoded nanoprobes have been reported [2,26,27]. Recently, we have demonstrated a SERS-fluorescence joint

* Corresponding authors.
E-mail addresses: wangzy@seu.edu.cn (Z. Wang), cyp@seu.edu.cn (Y. Cui).

0039-9140/$ - see front matter © 2013 Elsevier B.V. All rights reserved.
http://dx.doi.org/10.1016/j.talanta.2013.10.057

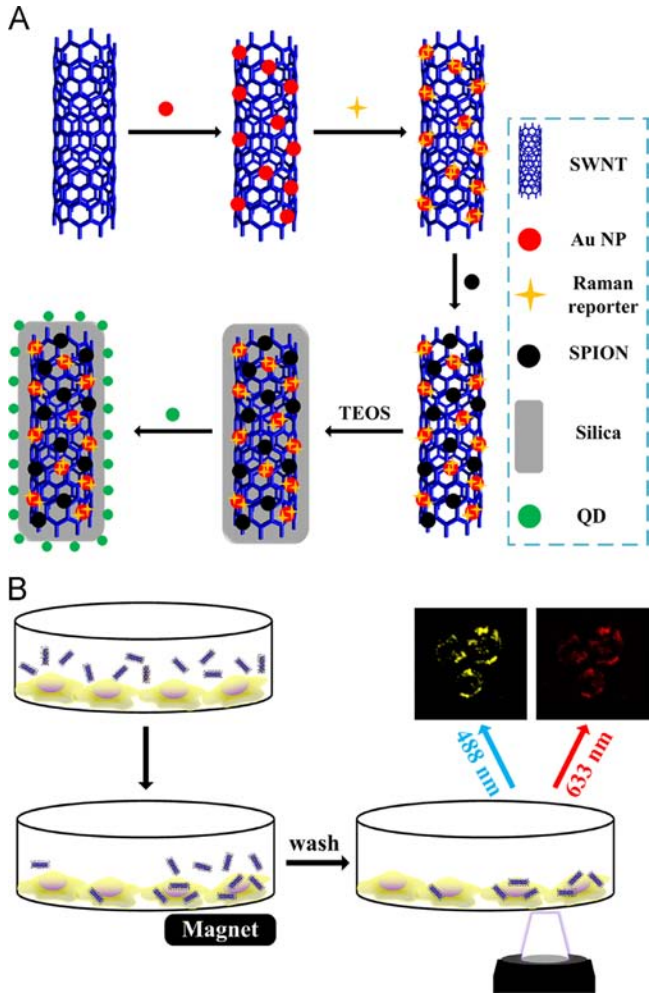

Scheme 1. (A) Fabrication procedures of the multifunctional nanoprobe. (B) Magnetic field guided SERS-fluorescence dual mode imaging of living cells.

spectral encoding (SFJSE) method using nanoprobes composed of metal NPs, silica and quantum dots (QDs). Such SFJSE based nanoprobes can be fruitfully employed in high-throughput bioanalysis [28].

Here, we present a new kind of SERS and fluorescence encoded magnetic nanoprobe for cell imaging. The structure of the nanoprobe is illustrated in Scheme 1A. Basically, single walled carbon nanotube (SWNT) is used as the building scaffold since it can provide numerous anchor spots for smaller NPs. SPIONs and Au NPs are electrostatically adsorbed onto the SWNT. The Au NPs are used as the SERS substrate and Raman molecules are linked to these Au NPs to generate SERS signals. Then a silica shell is coated to bury the Au NPs and SPIONs inside. Finally, CdSe/ZnS core–shell QDs are adsorbed to the silica shell to produce fluorescence signals, thus the multifunctional nanoprobe is obtained. *In vitro* experiments using human breast cancer cells (SKBR3 and MCF7) as the model cells confirm that the presented nanoprobe can realize magnetic field guided SERS and fluorescence dual mode imaging of live cells.

2. Material and methods

2.1. Materials

Single walled carbon nanotubes (SWNTs) were purchased from Nanoport Co. Ltd. (Shenzhen, China). CdSe/ZnS core–shell quantum dots with emission peaked at 530 nm and 580 nm were purchased from Wuhan Jiayuan Quantum Dot Technological Development Co., Ltd. Hydrogen tetrachloroaurate(III) trihydrate ($HAuCl_4 \cdot 3H_2O$), tetraethoxysilane (TEOS), polyethyleneimine (PEI, Branched, M.W. 10000) and 4-aminothiophenol (4ATP) were purchased from Alfa Aesar. 3-mercaptopropionic acid (MPA) and 5, 5'-dithiobis (2-nitrobenzoic acid) (DTNB) were purchased from Sigma-Aldrich. Ammonia water, H_2SO_4, HCl and HNO_3 were purchased from Shanghai Zhongshi Chemical Co., Ltd. Absolute ethanol was purchased from Nanjing Chemical Reagent Co., Ltd. NaCl was purchased from Guangdong Xilong Chemical Co., Ltd. All the reagents were used as received. Deionized water (Millipore Milli-Q grade) with a resistivity of 18.2 MΩ/cm was used in all the experiments.

2.2. Fabrication of the multifunctional nanoprobe

Several kinds of NPs, which were employed as the building blocks of the nanoprobe, were prepared beforehand according to previously published literature, including Au NPs [29], SPIONs [30] and water soluble MPA capped CdSe/ZnS QDs [31].

To fabricate the nanoprobe, first, SWNTs were sonicated in a mixture of H_2SO_4 and HNO_3 (3:1) for 24 h and subsequently exposed to 1 M HCl [32,33]. Excess acids were removed by dialysis and the resultant SWNTs were vacuum dried and redispersed in deionized water. Next, 200 μL of SWNTs (0.5 mg/mL) was added to 5 mL of PEI solution (10 mg/mL in 0.5 M NaCl) and sonicated for 1 h. Excess PEI was removed by centrifugation (12000 rpm, 20 min) for at least 3 times. Then the PEI wrapped SWNTs (denoted as SWNT@PEI) were redispersed in 200 μL of deionized water and centrifuged at 3000 rpm for 20 min. The supernatant was collected and the precipitate containing severely aggregated SWNTs was abandoned. To adsorb Au NPs, 200 μL of SWNT@PEI was added to 20 mL of Au NPs and sonicated for 1 h. The mixture was subsequently centrifuged thrice at 3000 rpm for 20 min to remove redundant Au NPs. The precipitate (denoted as SWNT@Au) was dispersed in 1 mL of deionized water. In order to make these nanoprobes SERS active, 6 μL of the Raman reporter (4ATP or DTNB, 10 mM in ethanol) solution was added respectively to SWNT@Au and aged for 1 h. After that, SPIONs were adsorbed to the SWNT@Au following a procedure similar to the adsorption of Au NPs. 1 mL of the SERS tagged SWNT@Au was mixed with 5 mL of PEI (10 mg/mL in 0.5 M NaCl) and sonicated for 1 h. Centrifugation was conducted again to remove excess PEI and the precipitate (denoted as SWNT@Au@PEI) was dispersed in 5 mL of deionized water containing SPIONs (0.1 mg/mL). The mixture was sonicated for 1 h to allow the adsorption of SPIONs and excess SPIONs were removed also by centrifugation. The precipitate (denoted as SWNT@Au–SPION) was dispersed in 40 mL of absolute ethanol. Then a silica layer was coated on the SWNT@Au–SPION via the Stöber method [34]. 2 mL of deionized water, 10 μL of TEOS and 2 mL of ammonia water (25%) were added to the as-prepared 40 mL of SWNT@Au–SPION ethanol solution. The mixture was sonicated for 2 h and 10 μL of TEOS was added thereafter, followed by continuous sonication for 6 h and aging overnight to complete the growth of silica shell. Finally, the silica coated SWNT@Au–SPION (denoted as SWNT@Au–SPION@SiO_2) was collected by centrifugation and magnetic separation. The sediments were dispersed in 5 mL of deionized water. Before attaching CdSe/ZnS QDs, SWNT@Au–SPION@SiO_2 was first modified with PEI as follows. 1 mL of SWNT@Au–SPION@SiO_2 was added to 2 mL of PEI solution (10 mg/mL in 0.5 M NaCl) and sonicated for 1 h. Excess PEI was removed by centrifugation and the sediment (denoted as SWNT@Au–SPION@SiO_2@PEI) was dispersed in 1 mL of deionized water. Next, 1 mL of MPA capped QDs solution (2 μM) was added to 1 mL of the SWNT@Au–SPION@SiO_2@PEI. The mixture solution was shaken for 2 h to allow the attachment of

QDs. After removing unbound QDs by centrifugation twice at 3000 rpm 20 min, the supernatant was discarded and the precipitate was dispersed in 1 mL of deionized water. Thus the multifunctional nanoprobe was eventually obtained.

2.3. Cell culture and in vitro experiments

Human breast cancer cells (SKBR3 and MCF7) were purchased from China Type Culture Collection and cultured in medium (DMEM) under standard cell culture condition (5% CO_2, 37 °C). Media were supplemented with 10% fetal bovine serum (Biochrom) and 1% penicillin–streptomycin (Nanjing KeyGen Biotech. Co., Ltd.).

To examine the SERS and fluorescence performance of the nanoprobe inside living cells, SKBR3 cells and MCF7 cells were seeded into culture dish (Corning) and incubated for 24 h. Then the nanoprobe encoded with 4ATP or DTNB was added to the cell culture dish (volume ratio probe solution:culture media=1:3). Five hours later, the culture media were discarded and the culture dish was gently washed with PBS before the SERS and fluorescence measurements.

To test the magnetic field guided cell imaging ability of the nanoprobe, cells were seeded into culture dishes and incubated for 24 h. Then the nanoprobe solution was added to the cell culture dish (volume ratio probe solution:culture media=1:3). And a magnet was placed on one side of the culture dish as illustrated in Scheme 1B. 2 h later, the culture media were discarded and the culture dishes were gently washed with PBS before cell imaging measurements.

The cytotoxicity of the nanoprobe was examined by the MTT (3-(4, 5-dimethylthiazol-2-yl)-2, 5-diphenyltetrazolium bromide) assay. SKBR3 cells (10^4/mL) were seeded onto 96-well plate (100 μL/hole) and incubated for 24 h at 37 °C under a 5% CO_2 atmosphere. Then different amounts of the nanoprobes were added and the cells were further incubated for 36 h. After that, 50 μL of MTT solution (MTT buffer to dilution buffer 1:4) was added into each well and the plate was incubated for another 4 h. The reaction was terminated by adding 150 μL of DMSO after removing the supernatant medium. When the purple formazan crystals were dissolved by DMSO, the absorbance of the wells at 490 nm were measured with a microplate reader (Bio-Rad model 680). Cells incubated in the absence of nanoprobes were used as a control.

2.4. Instruments

Extinction spectra were measured by a Shimadzu UV-3600 PC spectrophotometer with quartz cuvettes of 1 cm path length. Photoluminescence emission spectra were measured by an Edinburg FLS920 spectrofluorimeter, the spectrum linewidth was 1.5 nm for the selected slit width at the excitation and emission of the spectrofluorimeter. Zeta potential was measured by a Malvern zetasizer (Nano-ZS90). Transmission electron microscope (TEM) images were obtained with an FEI Tecnai G^2T20 electron microscope operating at 200 kV. SERS and fluorescence measurements were performed with a confocal microscopy (FV 1000, Olympus). Fluorescent images of cells were recorded at 488 nm excitation and SERS spectra were obtained at 633 nm excitation. The laser power was 2.3 mW at the sample position. Rayleigh scattering light was removed by a holographic notch filter. The Raman scattering light was directed to an Andor shamrock spectrograph equipped with a charge-coupled device (CCD).

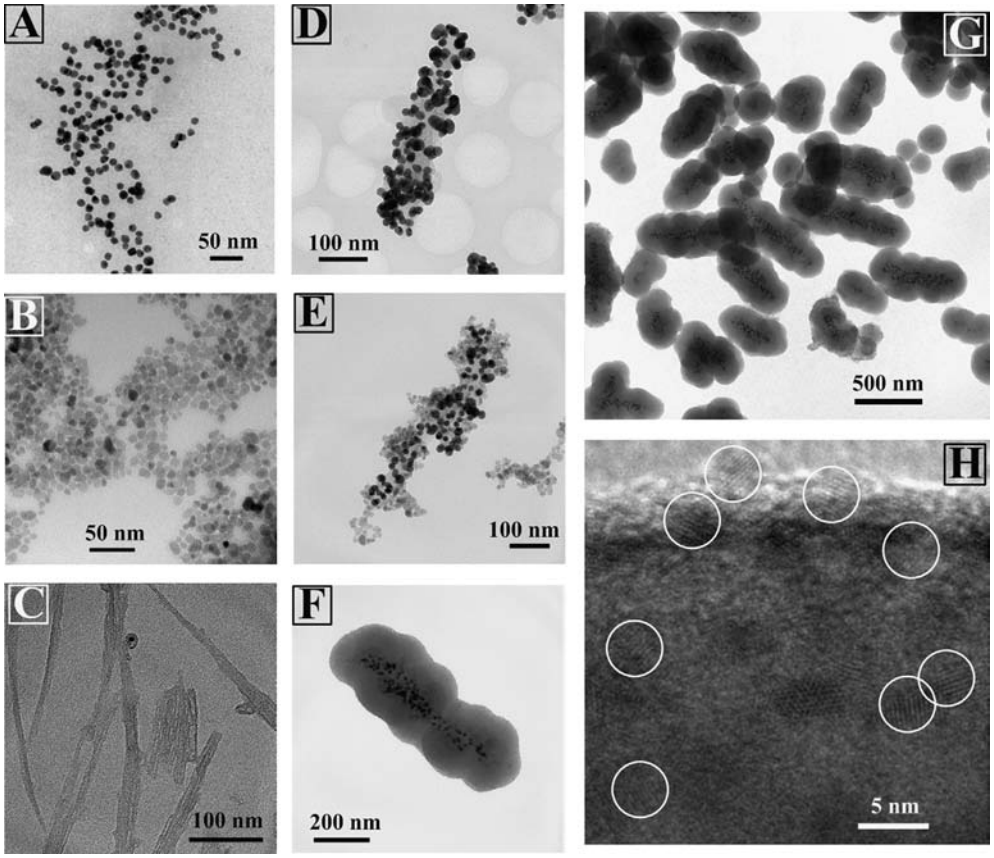

Fig. 1. TEM images of (A) Au NPs, (B) SPIONs, (C) SWNTs, (D) SWNT@Au, (E) SWNT@Au–SPION, (F) nanoprobe, (G) Large scale TEM image of the nanoprobes, and (H) HRTEM image of the nanoprobe surface, the white circles indicate CdSe/ZnS QDs.

3. Results and discussion

3.1. Morphological characterization of the nanoprobe

To construct the multifunctional nanoprobe, SWNTs are implicated as the building scaffold while Au NPs, SPIONs, and CdSe/ZnS QDs are used as the building blocks. TEM images of the Au NPs and SPIONs are shown in Fig. 1A and B. The average diameter of the Au NPs is nearly 13 nm while that of the SPIONs is 10 nm. Since the original SWNTs are tangled and water insoluble, they were oxidized and cut short by sonication in a mixture of H_2SO_4 and HNO_3 as described in the experimental section. After subsequent treatment with HCl, carboxyl groups were introduced to the sidewalls of SWNTs, rendering the SWNTs good water solubility [32,33]. Fig. 1C is the TEM image of the shortened SWNTs. The diameter of a single SWNT is approximately 2 nm while that of the SWNT bundles ranges from 10 to 28 nm. Au NPs and SPIONs were assembled onto the SWNTs through electrostatic interactions. The obtained water soluble SWNTs are negatively charged due to their surface carboxyl groups (Fig. 2(1)). To adsorb negatively charged Au NPs, SWNTs were first wrapped with branched cationic polymer PEI, which can introduce abundant amino groups onto the SWNT surface, resulting in high positive surface charge (Fig. 2(2)). The TEM image of the Au NPs assembled SWNTs (denoted as SWNT@Au) is shown in Fig. 1D, which clearly demonstrates that many Au NPs have been adsorbed onto the SWNTs. SERS signals were integrated by mixing Raman active molecules (DTNB or 4ATP) with SWNT@Au. These molecules can covalently link to the Au NPs via Au–S bonds. The SWNT@Au is negatively charged due to the Au NPs (Fig. 2(3)). Before attaching SPIONs, the surface charge of SWNT@Au was reversed by another round of PEI wrapping (Fig. 2(4)). Then the SPIONs were adsorbed and the TEM image of SPIONs and Au NPs attached SWNTs (denoted as SWNT@Au–SPION) is shown in Fig. 1E. As can been seen, the dark particles on the SWNT are Au NPs while the light gray ones are SPIONs. Zeta potential measurement result also proved that the SPIONs have been successfully adsorbed since the SWNT@Au–SPION exhibited a negative surface charge. Next, a silica shell was introduced via the Stöber method to bury the SWNT@Au–SPION inside and ensure that the Au NPs and SPIONs would not fall off from the SWNTs. The silica shell also plays another vital role that is to provide isolation between QDs and the inner SWNT@Au–SPION, because the fluorescence of QDs can be quenched by SWNTS, Au NPs and SPIONs. MPA capped water soluble CdSe/ZnS QDs were also anchored onto the silica coated SWNT@Au–SPION (denoted as SWNT@Au–SPION@SiO_2) via electrostatic interaction. The SWNT@Au–SPION@SiO_2 is negatively charged due to the silica shell (Fig. 2(6)). So PEI wrapping is a necessity before adsorbing QDs (Fig. 2(7)). When CdSe/ZnS QDs were eventually anchored, the multifunctional nanoprobe was obtained and its TEM images were demonstrated in Fig. 1F and G. The nanoprobe has a cylinder morphology due to the SWNT scaffold. The diameter of the nanoprobe is about 300 nm while the length ranges from 400 nm to 1 μm. The diversity in length mainly

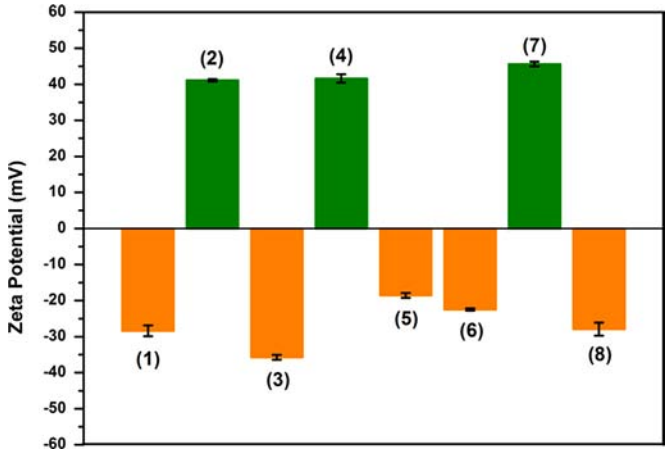

Fig. 2. Zeta potential obtained during the fabrication of the nanoprobe. (1) SWNT, (2) SWNT@PEI, (3) SWNT@Au, (4) SWNT@Au@PEI, (5) SWNT@Au–SPION, (6) SWNT@Au–SPION@SiO_2, (7) SWNT@Au–SPION@SiO_2@PEI, and (8) nanoprobe. The error bars represent the standard deviation of 3 measurements.

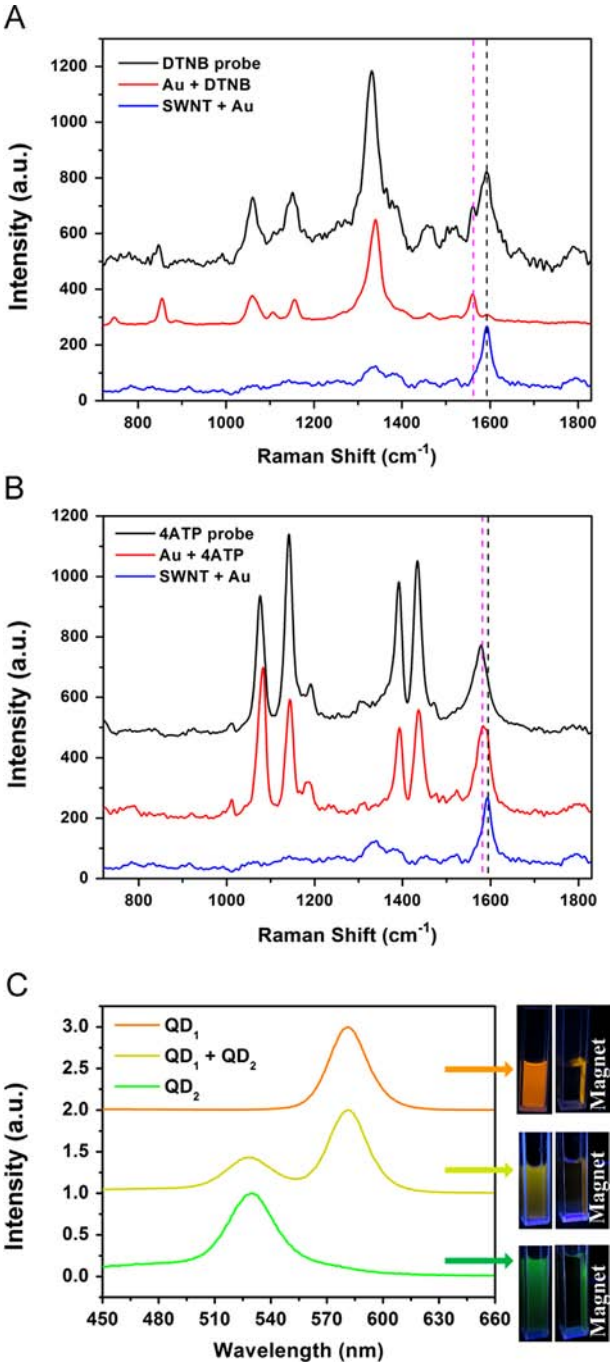

Fig. 3. (A) SERS spectra of the nanoprobes encoded with DTNB, SWNT@Au and DTNB adsorbed solely on Au NPs. (B) SERS spectra of the nanoprobes encoded with 4ATP, SWNT@Au and 4ATP adsorbed solely on Au NPs. (C) Fluorescence spectra of the nanoprobes encoded with QD_1, QD_2 or both QD_1 and QD_2. The photographs of the nanoprobes illuminated under 365 nm UV light in the presence or absence of a magnet are also shown. (For interpretation of the references to color in this figure, the reader is referred to the web version of this article.)

originates from the heterogeneous nature of SWNTs [35]. Fig. 1H is enlarged high resolution TEM (HRTEM) image of the nanoprobe surface, which clearly shows the lattice of the attached CdSe/ZnS QDs as indicated by white circles. The above results confirmed that the fabricated nanoprobe has a structure as expected. Besides, considering the stability of the nanoparticles, our result shows that the nanoparticles kept their stability within 24 h. After an even longer time, the nanoparticles tended to precipitate due to their relative large sizes. However, the precipitate can be easily redispersed in water by hand shaking.

3.2. SERS and fluorescence performance of the nanoprobe

The presented nanoprobe is encoded with both SERS and fluorescence signals. SERS signal is generated by attaching Raman reporter molecules to the Au NPs. As a proof-of-concept experiment, two Raman molecules were employed in the experiments, i.e. DTNB and 4ATP. Fig. 3A shows the SERS spectrum of the nanoprobe encoded with DTNB. The SERS bands of DTNB have been well assigned in previously published literatures [36]. The strong peak at 1333 cm^{-1} is assigned to the symmetric stretch of the nitro groups. The band at 847 cm^{-1} is attributed to the nitro scissoring vibration. And the band at 1558 cm^{-1} is assigned to the aromatic ring C–C stretching modes. Besides, the band at 1063 cm^{-1} is probably a succinimidyl N–C–O stretch overlapping with aromatic ring modes. There is a marked difference between the SERS spectrum of the nanoprobe and that of DTNB adsorbed solely on Au NPs (Fig. 3A, red curve), that is, the emergence of the new band at 1590 cm^{-1}. By examining the SERS spectrum of SWNT@Au before the addition of Raman reporter (Fig. 3A, blue curve), it is obvious that the 1590 cm^{-1} band is the inherent G-band of SWNTs enhanced by the attached Au NPs [37,38]. While for 4ATP encoded nanoprobe, the Raman bands at 1007 cm^{-1}, 1076 cm^{-1}, 1190 cm^{-1}, and 1576 cm^{-1} are assigned to the a_1 modes while those at 1142 cm^{-1}, 1390 cm^{-1}, and 1432 cm^{-1} are assigned to the b_2 modes (Fig. 3B) [39]. Although the origination of the b_2 mode Raman bands of 4ATP is controversial, 4ATP is used here because it can produce strong SERS signals [40–42]. In Fig. 3B, the G-band of SWNTs is barely seen in the SERS spectrum of the nanoprobe because of its overlap with the 1576 cm^{-1} band of 4ATP.

As for fluorescence, CdSe/ZnS QDs are used as the fluorescent agent due to their narrow emission bandwidth, high quantum yield and good photo-stability compared with organic fluorophores. The original CdSe/ZnS QDs were transferred to water phase by ligand exchange using MPA according to previously published literature [31]. The MPA capped CdSe/Zn QDs were anchored on the outmost surface of the nanoprobe via electrostatic interaction and isolated from the inner SWNT@Au–SPION core with a silica shell. In the experiments, two batches of CdSe/Zn QDs with emission peaked at 580 nm (QD_1) and 530 nm (QD_2) were used. Fig. 3C shows the fluorescence spectra of the nanoprobe encoded with different QDs. The fluorescence of QD_1 or QD_2 was well retained in the nanoprobe. When a mixture of QD_1 and QD_2 (molar ratio 1:2) was used in the final QDs adsorption step, both QD_1 and QD_2 were simultaneously attached on a single nanoprobe and another fluorescence spectrum was obtained as shown in Fig. 3C (middle curve). When the nanoprobes encoded with different QDs (i.e. different fluorescence signals) were illuminated by a UV-light, they gave bright photoluminescence (Fig. 3C). Aside from the encoded SERS and fluorescence signals, the nanoprobes also incorporate SPIONs, which allow them to be magnetically controlled by an external magnet. As shown in the photograph in Fig. 3C, with a magnet present, the nanoprobes dispersed in deionized water were quickly accumulated within 2 min, resulting in bright luminescent precipitates containing the nanoprobes and a clear water solution. Collectively, the above results indicate that the fluorescent, magnetic and SERS active nanoprobe has been successfully fabricated.

3.3. In vitro cell imaging experiments

To evaluate the cell imaging ability of the nanoprobe, SKBR3 cells and MCF7 cells were used as the model cells. Before the imaging experiments, the stability of the nanoparticles in cell media was checked. The result shows that our probe has a good stability in the media and the QDs were still coated on the surfaces of the nanoprobes. Then, SKBR3 cells were incubated with the

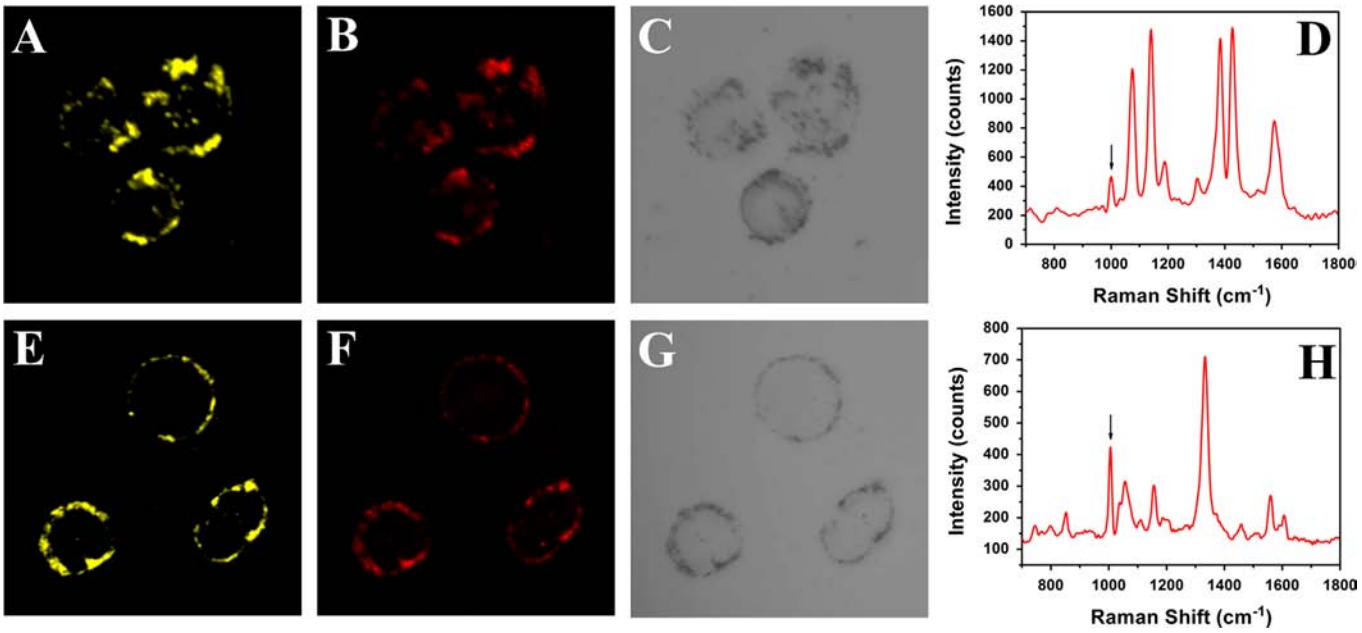

Fig. 4. (A–D) SKBR3 cells incubated with 4ATP encoded nanoprobe, (A) fluorescence image, (B) SERS image, (C) bright field image, (D) SERS spectrum obtained from these SKBR3 cells. (E–H) MCF 7 cells incubated with DTNB encoded nanoprobe, (E) fluorescence image, (F) SERS image, (G) bright field image, (H) SERS spectrum obtained from these MCF7 cells. The peak indicated by an arrow in the SERS spectra belongs to the culture dish.

4ATP and QD_1 encoded nanoprobes for 5 h to allow sufficient cellular uptake of the nanoprobe, and MCF7 cells were incubated with the DTNB and QD_1 encoded ones. In the experiments, the emission lights belong to the fluorescence of QD_1 within the range of 560–600 nm were collected under 488 nm excitation, while the SERS lights within the range of 660–710 nm were collected using 633 nm excitation. In this way, fluorescence and SERS dual mode imaging of the cells can be readily achieved simply by changing the excitation wavelengths. Fig. 4 demonstrates the cell imaging results. The nanoprobes incorporated by the cells can clearly be observed as black dots in the bright field images (Fig. 4C and G). The fluorescence and SERS signals were well maintained when the nanoprobes were taken up by live cells and were strong enough to fulfill dual mode cell imaging (Fig. 4A, B, E and F). The SERS spectra obtained from these SKBR3 cells and MCF7 cells are also shown in Fig. 4D and H, which clearly demonstrate the representative Raman bands of 4ATP and DTNB, respectively. The results indicate that the proposed nanoprobe is capable of keeping their distinct SERS and fluorescence performance after being taken up by living cells and thus can be employed as a live cell imaging agent.

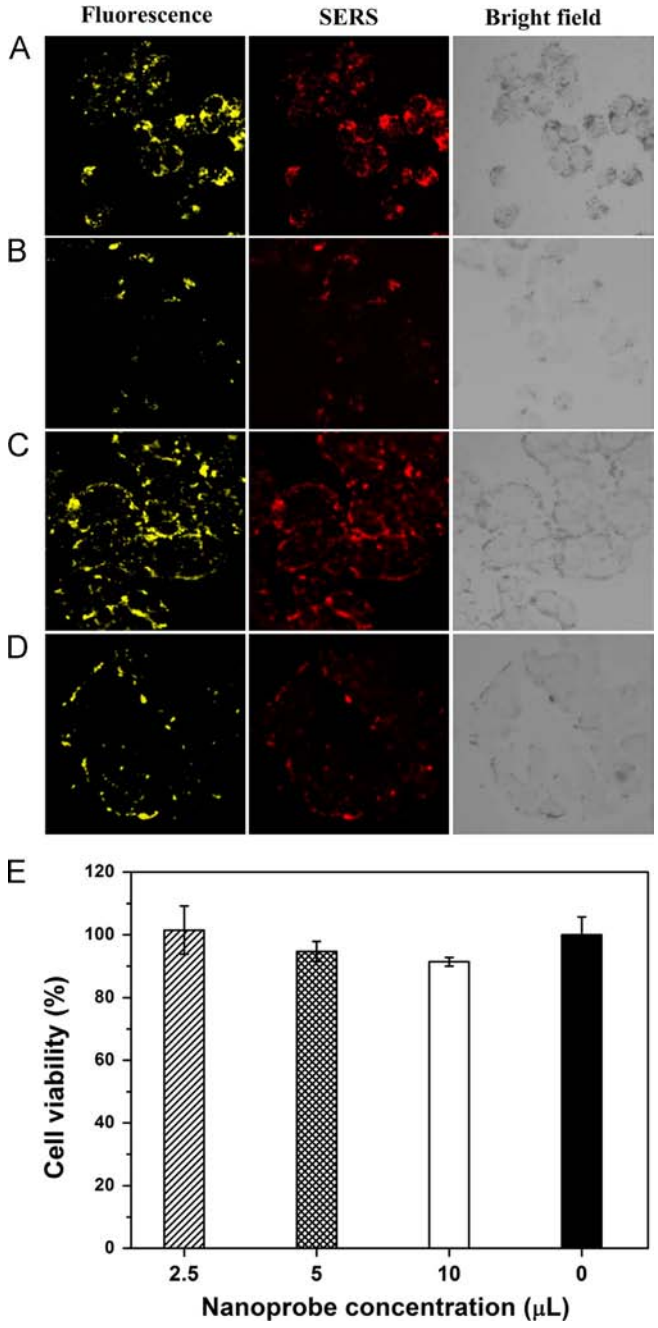

Fig. 5. (A, B) SKBR3 cells incubated with 4ATP encode nanoprobe near (A) or away (B) from the magnet. (C, D) MCF7 cells incubated with DTNB encode nanoprobe near (C) or away (D) from the magnet. (E) Viability of SKBR3 cells incubated with the nanoprobes.

Another special property of the presented nanoprobe is its magnetism provided by the SPIONs, which allows it to be remotely manipulated by an external magnetic field. To examine the potential application of the nanoprobe in magnetic field guided specific cell imaging, nanoprobes were added to the cell culture dish with a magnet placed on one side (as shown in Scheme 1B). After incubation for 2 h, the cells were subjected to SERS and fluorescence measurements. The results were shown in Fig. 5. Fig. 5A belongs to SKBR3 cells adhering near the magnet side while Fig. 5B belongs to those far from the magnet side in the same culture dish. Obviously, cells near the magnet exhibited markedly stronger fluorescence and SERS signals than those away from the magnet. This is rational because the nanoprobes suspended in the culture medium were gradually accumulated by the magnet. Thus cells near the magnet were actually exposed to a higher concentration of nanoprobes, resulting in more efficient cellular uptake. The higher cellular uptake near the magnet side was also confirmed by the bright field images, as more black dots (nanoprobes) appeared on these cells compared to those away from the magnet (Fig. 5). Similar results were observed using MCF7 cells (Fig. 5C and D). Consequently, the nanoprobe can indeed accomplish magnetic field guided dual mode live cell imaging. Furthermore, MTT assay was conducted to examine the biocompatibility of the presented nanoprobe. The results shown in Fig. 5E indicate that the nanoprobe exhibits a negligible cytotoxicity as the cell viabilities corresponding to different nanoprobe concentrations were more than 90%. The good biocompatibility of the nanoprobe is very beneficial for live cell imaging applications.

4. Conclusions

In summary, we have successfully designed and fabricated a multifunctional magnetic nanoprobe with optically encoded signals for live cell imaging. SWNTs with large surface areas were used as the building scaffold, Au NPs, SPIONs and CdSe/ZnS QDs were implicated as the building blocks. Experimental results proved that the proposed nanoprobe can produce strong fluorescence and SERS signals under different excitation wavelengths. And its magnetism provided by SPIONs allows it to realize magnetic field guided dual mode live cell imaging. The encoded fluorescence and SERS signals can easily be changed using different Raman reporters or QDs, resulting in what we have previously reported as SFJSE, thus a more fabulous multiplex ability can be obtained with the nanoprobes [28]. In addition to live cell imaging, other potential applications of this kind of multifunctional nanoprobe include optical coding, highly sensitive biosensing and so on. Besides, the nanoprobe can further be combined with other materials (e.g. liposomes, peptides, etc.) to build an optically traceable and magnetically controllable drug delivery vehicle, which may have a great potential in improving drug delivery efficiency.

Acknowledgment

This work was supported by the Natural Science Foundation of China (NSFC) (Nos. 61275182, 61177033, and 21104009), Science Foundation for The Excellent Youth Scholars of Southeast University, the Scientific Research Foundation of Graduate School

of Southeast University (YBJJ1125), the Scientific Innovation Research Foundation of College Graduate in Jiangsu Province (CXZZ12_0094) and the Fundamental Research Funds for the Central Universities.

References

[1] M. Liong, J. Lu, M. Kovochich, T. Xia, S.G. Ruehm, A.E. Nel, F. Tamanoi, J.I. Zink, Acs Nano 2 (2008) 889–896.
[2] Z. Wang, S. Zong, J. Yang, J. Li, Y. Cui, Biosens. Bioelectron. 26 (2011) 2883–2889.
[3] L. Li, C. Liu, L. Zhang, T. Wang, H. Yu, C. Wang, Z. Su, Nanoscale 5 (2013) 2249–2253.
[4] X. Ma, X. Wang, M. Zhou, H. Fei, Adv. Healthc. Mater., (2013) http://dx.doi.org/10.1002/adhm.201300037.
[5] S. Zhang, Z. Chu, C. Yin, C. Zhang, G. Lin, Q. Li, J. Am. Chem. Soc. 135 (2013) 5709–5716.
[6] X. Kang, Z. Cheng, D. Yang, P.a. Ma, M. Shang, C. Peng, Y. Dai, J. Lin, Adv. Funct. Mater. 22 (2012) 1470–1481.
[7] M.H. Cho, E.J. Lee, M. Son, J.-H. Lee, D. Yoo, J.-w. Kim, S.W. Park, J.-S. Shin, J. Cheon, Nat. Mater. 11 (2012) 1038–1043.
[8] B. Kang, J. Li, S. Chang, M. Dai, C. Ren, Y. Dai, D. Chen, Small 8 (2012) 777–782.
[9] M. Liu, L. Gan, L. Chen, Z. Xu, D. Zhu, Z. Hao, L. Chen, Langmuir 28 (2012) 10725–10732.
[10] A.K. Singh, W. Lu, D. Senapati, S.A. Khan, Z. Fan, T. Senapati, T. Demeritte, L. Beqa, P.C. Ray, Small 7 (2011) 2517–2525.
[11] Y.P. Sun, K.F. Fu, Y. Lin, W.J. Huang, Acc. Chem. Res. 35 (2002) 1096–1104.
[12] Z. Liu, K. Chen, C. Davis, S. Sherlock, Q. Cao, X. Chen, H. Dai, Cancer Res. 68 (2008) 6652–6660.
[13] R. Singhal, Z. Orynbayeva, R.V.K. Sundaram, J.J. Niu, S. Bhattacharyya, E.A. Vitol, M.G. Schrlau, E.S. Papazoglou, G. Friedman, Y. Gogotsi, Nat. Nanotechnol. 6 (2011) 57–64.
[14] Z. Chen, S.M. Tabakman, A.P. Goodwin, M.G. Kattah, D. Daranciang, X. Wang, G. Zhang, X. Li, Z. Liu, P.J. Utz, K. Jiang, S. Fan, H. Dai, Nat. Biotechnol. 26 (2008) 1285–1292.
[15] N.H. Levi-Polyachenko, E.J. Merkel, B.T. Jones, D.L. Carroll, J.H. Stewart, Mol. Pharmcol. 6 (2009) 1092–1099.
[16] A.L. Antaris, J.T. Robinson, O.K. Yaghi, G. Hong, S. Diao, R. Luong, H. Dai, Acs Nano 7 (2013) 3644–3652.
[17] P. Dames, B. Gleich, A. Flemmer, K. Hajek, N. Seidl, F. Wiekhorst, D. Eberbeck, I. Bittmann, C. Bergemann, T. Weyh, L. Trahms, J. Rosenecker, C. Rudolph, Nat. Nanotechnol. 2 (2007) 495–499.
[18] Y. Namiki, T. Namiki, H. Yoshida, Y. Ishii, A. Tsubota, S. Koido, K. Nariai, M. Mitsunaga, S. Yanagisawa, H. Kashiwagi, Y. Mabashi, Y. Yumoto, S. Hoshina, K. Fujise, N. Tada, Nat. Nanotechnol. 4 (2009) 598–606.
[19] J.-H. Lee, K. Lee, S.H. Moon, Y. Lee, T.G. Park, J. Cheon, Angew. Chem. Int. Ed. 48 (2009) 4174–4179.
[20] J. Guo, W. Yang, C. Wang, J. He, J. Chen, Chem. Mater. 18 (2006) 5554–5562.
[21] J. Gao, G. Liang, J.S. Cheung, Y. Pan, Y. Kuang, F. Zhao, B. Zhang, X. Zhang, E.X. Wu, B. Xu, J. Am. Chem. Soc. 130 (2008) 11828–11833.
[22] Z. Wang, H. Wu, C. Wang, S. Xu, Y. Cui, J. Mater. Chem. 21 (2011) 4307–4313.
[23] S. Zong, Z. Wang, R. Zhang, C. Wang, S. Xu, Y. Cui, Biosens. Bioelectron. 41 (2013) 745–751.
[24] L. Lin, X. Tian, S. Hong, P. Dai, Q. You, R. Wang, L. Feng, C. Xie, Z.-Q. Tian, X. Chen, Angew. Chem. Int. Ed. 52 (2013) 7266–7271.
[25] C.L. Zavaleta, E. Garai, J.T.C. Liu, S. Sensarn, M.J. Mandella, D. Van de Sompel, S. Friedland, J. Van Dam, C.H. Contag, S.S. Gambhir, Proc. Natl. Acad. Sci. 110 (2013) E2288–E2297.
[26] Y. Cui, X.-S. Zheng, B. Ren, R. Wang, J. Zhang, N.-S. Xia, Z.-Q. Tian, Chem. Sci. 2 (2011) 1463–1469.
[27] S. Lee, H. Chon, S.-Y. Yoon, E.K. Lee, S.-I. Chang, D.W. Lim, J. Choo, Nanoscale 4 (2012) 124–129.
[28] Z. Wang, S. Zong, W. Li, C. Wang, S. Xu, H. Chen, Y. Cui, J. Am. Chem. Soc. 134 (2012) 2993–3000.
[29] G. FRENS, Nat. Phys. Sci. 241 (1973) 20–22.
[30] D. Yang, J. Hu, S. Fu, J. Phys. Chem. C 113 (2009) 7646–7651.
[31] B.-K. Pong, B.L. Trout, J.-Y. Lee, Langmuir 24 (2008) 5270–5276.
[32] J. Chen, M.A. Hamon, H. Hu, Y.S. Chen, A.M. Rao, P.C. Eklund, R.C. Haddon, Science 282 (1998) 95–98.
[33] K.A. Williams, P.T.M. Veenhuizen, B.G. de la Torre, R. Eritja, C. Dekker, Nature 420 (2002) (761–761).
[34] C. Graf, D.L.J. Vossen, A. Imhof, A. van Blaaderen, Langmuir 19 (2003) 6693–6700.
[35] W. Yang, K.R. Ratinac, S.P. Ringer, P. Thordarson, J.J. Gooding, F. Braet, Angew. Chem. Int. Ed. 49 (2010) 2114–2138.
[36] D.S. Grubisha, R.J. Lipert, H.Y. Park, J. Driskell, M.D. Porter, Anal. Chem. 75 (2003) 5936–5943.
[37] L. Zhang, Z. Jia, L. Huang, S. O'Brien, Z. Yu, J. Phys. Chem. C 111 (2007) 11240–11245.
[38] C. Zavaleta, A. de la Zerda, Z. Liu, S. Keren, Z. Cheng, M. Schipper, X. Chen, H. Dai, S.S. Gambhir, Nano Lett. 8 (2008) 2800–2805.
[39] M. Osawa, N. Matsuda, K. Yoshii, I. Uchida, J. Phys. Chem. 98 (1994) 12702–12707.
[40] Y.-F. Huang, H.-P. Zhu, G.-K. Liu, D.-Y. Wu, B. Ren, Z.-Q. Tian, J. Am. Chem. Soc. 132 (2010) 9244–9246.
[41] H.-K. Choi, H.K. Shon, H. Yu, T.G. Lee, Z.H. Kim, J. Phys. Chem. Lett. 4 (2013) 1079–1086.
[42] K. Kim, K.L. Kim, K.S. Shin, J. Phys. Chem. C 117 (2013) 5975–5981.